# CHAPTER 3 DATA SETS AND METHODOLOGY

Basically, knowledge of the consolidation, thermo-physical properties, state of alteration, thickness, and mineralogy of ILDs may provide details about their origin and evolution.

ILDs are characterised by the following parameters:

- Morphology
- Albedo
- Elevation
- Thickness
- Consolidation of materials
- Mineralogy
- Layering geometry

To examine these, data sets of the following missions were used.

## *3.1 DATA SETS*

Due to its specific capabilities in order to serve the above named parameters, data of the following instruments on Martian missions have been used to support the analyses of the ILDs.

### 3.1.1 HRSC

***HRSC***[1] (*High Resolution Stereo Camera; Neukum and Jaumann*, 2004; *Jaumann et al.,* 2007; *The HRSC Co-Investigator Team et al.*, 2007) data from the Mars Express (MEX) mission launched in 2003 have been used in this study.
The camera is imaging the entire planet in stereo and four colours with a resolution of up to 10 metres. Selected areas are imaged at < 5-metre resolution using the super resolution channel (SRC). The camera's greatest strength is its unprecedented targeting accuracy, achieved by combining images of two different channels, and the stereo capability (Fig. 15) providing 3D images, which reveal the topography of Mars in full colour [*Jaumann et al.*, 2007].

[1] http://berlinadmin.dlr.de/Missions/express/indexeng.shtml (image credit for all HRSC images: ESA/DLR/FUB G. Neukum)

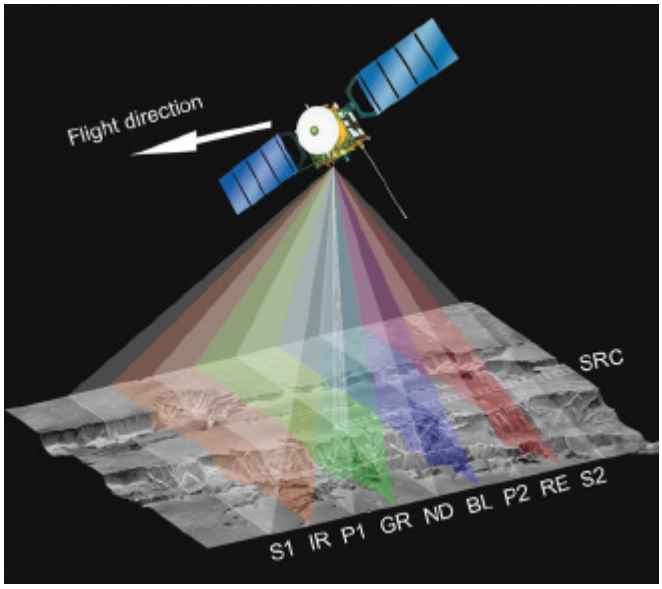


**Figure 15:** HRSC mode of operation. Nine photosensitive CCD rows operate perpendicular to the flight direction, scanning the surface line by line. ND - nadir channel; S1, S2 - stereo 1 and stereo 2 (±18.9°); P1, P2 - photometry 1 and photometry 2 (±12.8°); IR - near infrared channel (±15.9°); GR - green channel (±3.3°); BL - blue channel (-3.3°); RE - red channel (-15.9°). All nine line sensors have a cross-track field of view of ±6°. SRC - super resolution channel (panchromatic; *Jaumann et al.*, 2007).

### 3.1.2 MOLA

***MOLA***[2] *(Mars Orbiter Laser Altimeter;* MOLA-2; *Smith et al.*, 2001) launched in 1996 on the Mars Global Surveyor (MGS) mission provided further data. It is a laser altimeter with a range precision of 37 cm and a profiling ground resolution of the Martian surface of ~300 m. The instrument's purpose is to generate a topographical map of Mars. The vertical accuracy of the instrument is limited by orbit determination, reaching ~2 m.

### 3.1.3 MOC

***MOC***[3] *(Mars Orbiter Camera)* launched in 1996 on the Mars Global Surveyor[4] mission – MGS - [*Malin et al.*, 1992; *Malin and Edgett*, 2001] consists of 3 instruments: a narrow angle camera (MOC-NA) for grey-scale (black and white) high resolution images (spatial resolution 1.4 to 12 m/ pixel), and two wide angle cameras for atmospheric studies and geological context (spatial resolution < 240 m/ pixel) and for daily global imaging (7.5 km/pixel). The narrow angle camera takes images of the entire planet through time to enable research into temporal changes in the atmosphere and on the surface.

[2] http://mola.gsfc.nasa.gov/
[3] http://www.msss.com/mgs/moc/index.html
[4] http://mars.jpl.nasa.gov/missions/past/globalsurveyor.html

### 3.1.4 HiRISE

***HiRISE***[5] (*High Resolution Imaging Science Experiment*; *McEwen et al.*, 2007) data from the Mars Reconnaissance Orbiter[6] (MRO) mission launched in 2005 were used for detailed (small-scale) 2D analyses, providing images and spectral information. As one of the orbiter's cameras, it is the largest ever flown on a planetary mission.

### 3.1.5 TES

***TES***[7] (*Thermal Emission Spectrometer*; *Christensen et al.*, 2001a) on the Mars Global Surveyor (MGS) mission launched in 1996 measured the thermal infrared energy (heat) emitted from Mars to obtain information about its geology, atmosphere, and composition.

### 3.1.6 THEMIS

***THEMIS***[8] (*Thermal Emission Imaging Spectrometer)* data on the Mars Odyssey (MO) spacecraft launched 2001 provided data which enabled the development of a global map of chemical elements occurring on the surface.
THEMIS [*Christensen et al.*, 2004] analyses the visual (VIS) and infrared (IR) bands of the electromagnetic spectrum. It combines a 5-wavelength visual with a 9-wavelength infrared imaging system. The IR and VIS subsystems have resolutions of 100 m/ pixel and 19 m/ pixel, respectively [*Christensen et al.*, 2004], providing spectral information which helps to understand the geological processes that formed the surface.

### 3.1.7 OMEGA

***OMEGA***[9] (*Observatoire pour la Minéralogie, l'Eau, les Glaces et l'Activité* ; *Bibring et al.*, 2004) is on board the Mars Express (MEX) spacecraft[10] launched in 2003. The instrument maps the surface composition in 100-metre squares. It determines the mineral compositions in the visible and infrared light reflected from the Martian surface in wavelengths from 0.5 – 5.2 microns. As the light reflected from the surface has to pass through the atmosphere before entering the instrument, OMEGA also measures aspects of the atmospheric composition.
OMEGA-data provide information about the iron content, water content, and hydration state of rocks and clay minerals, as well as the abundance of non-silicate minerals like

[5] http://marsoweb.nas.nasa.gov/HiRISE/instrument.html
[6] http://mars.jpl.nasa.gov/mro
[7] http://tes.la.asu.edu
[8] http://themis.asu.edu
[9] http://www.ias.u-psud.fr/website/modules/content_pla/index.php?id=14
[10] http://www.esa.int/SPECIALS/Mars_Express/index.html

carbonates and nitrates [*Bibring et al.*, 2004]. As minerals form under specific conditions, their detection reveals the environmental conditions and the climate prevailing at a given time.

### 3.1.8 CRISM

***CRISM***[11] (*Compact Reconnaissance Imaging Spectrometer for Mars; Murchie et al.*, 2003; *Murchie et al.*, 2004; *Silverglate and Fort*, 2004; *Silverglate et al.*, 2004; *Murchie et al.*, 2007) on the Mars Reconnaissance Orbiter[12] (MRO) mission provided data that were used within a collaboration framework. The instrument detects water-related minerals on Mars, covering the whole planet at a resolution of 200 metres but in addition allows precise targeting with a spatial resolution up to 15-19 m/px.
It discovers aqueous and hydrothermal deposits and maps the geology, composition and stratigraphy of surface features. The instrument looks for seasonal variations in Martian dust and ice aerosols, as well as in the water content of surface materials in order to develop a new understanding of the climate. Compared to OMEGA, CRISM has a higher spatial resolution and therefore targets are detected more precisely.

## *3.2 DATA BASIS*

HRSC data form the basis for ILD characterisation. HRSC nadir images of ILDs were first identified and captured on a spreadsheet, quoting the name, latitude and longitude of the exposure. ILD parameters were then added over time.
The main part of the data (ASCII- and raster data sets) was processed using the DLR VICAR[13], ISIS[14] and IDL[15] software to gain information out of image, elevation and spectral data. Most of the data were then formatted to ESRI[16] *ArcGIS*-files.
ESRI ArcGIS (geographic information system) was the main workspace. It is very helpful for capturing, storing, analyzing, managing, and presenting data that are spatially referenced by location links. All data were combined in that system. A global MOLA map was used for improved demonstration and orientation, so that various data sets from different missions were applied (Table 6).

[11] http://crism.jhuapl.edu/ (images credit for all CRISM images: NASA)
[12] http://mars.jpl.nasa.gov/mro (images credit for all HiRISE images: NASA)
[13] *VICAR: Video Image Communication And Retrieval (JPL, Pasadena/ USA)*
[14] *ISIS: Integrated Software for Imaging Spectrometers (USGS, USA)*
[15] *IDL: Interactive Data Language*
[16] *ESRI: Environmental Systems Research Institute*

**Table 8:** Overview of the datasets that were used to characterise ILDs. The spatial resolutions correspond to the ones that were used. For information on the mineralogy, published OMEGA-data and CRISM-data within the scope of collaboration were used.

| Dataset | Mission | Number of Channels, Spectral Range | Spatial Resolution/px | Data Type | Relevance, Coverage |
|---|---|---|---|---|---|
| HRSC | Mars Express | 4 (colour) + 5 (panchromatic), 440-970 nm | nadir: 12.5-50 m DTM: 50-175 m (vertical precision: 12.5-50 m) | Raster (optical image and elevation data) | Data basis, data for every locality |
| MOLA | Mars Global Surveyor | | MOLA DEMs (DLR): 463 m (vertical precision ~2 m) | ASCII, raster (elevation data) | regional context map |
| MOC | Mars Global Surveyor | | 2.8 m | Raster (optical image data) | NA data for every locality if available |
| HiRISE | Mars Reconnaissance Orbiter | 3 (colour), ~536-874 nm | 25 cm | raster (optical image data) | data for every locality if available |
| THEMIS | Mars Odyssey | 5 VNIR: 0.42-0.86 µm 9 TIR: 6.78–14.88 µm | 100 m (IR[2]) | raster (thermal image data) | data for every locality if available |
| TES | Mars Global Surveyor | interferometer: 5.8-50 µm radiometer: 5.1-150 µm and 0.3-2.9 µm | 3 km | ASCII (thermal data) | data for every locality |
| OMEGA | Mars Express | 352, 0.35-5.1 µm | 0.3-3 km | ASCII[1], raster | data[17] for every locality, if available |

[17] *Gendrin et al.* [2005], *Glotch and Rogers* [2007], *NoeDobrea et al.* [2008]

| | | | | | |
|---|---|---|---|---|---|
| CRISM | Mars Reconnaissance Orbiter | 544, 0.392-3.92 µm | 15-20 m | raster (spectral image data) | data for every locality, if available |

In combination, these data sets permit detailed studies of ILDs and may serve to identify the processes that were involved in their formation.

## 3.2 *DATA ANALYSIS APPROACH AND INTERPRETATION*

### 3.2.1 Photogeology

HRSC-data (Sect. 3.1.1, Table 8) formed the basis for ILD characterisation. 2D-nadir and false colour images were mainly used to describe the albedo of ILDs and their morphologies. MOC and HiRISE-images (Sect. 3.1.2, 3.1.4, Table 8) were applied to describe more small-scale features such as the surface morphology and consolidation of materials. Image datasets were combined into spectral and elevation data to generate stratigraphic profiles of each ILD in order to establish whether there are comparable stratigraphic units that potentially correlate.

Morphology

Generally, HRSC orthoimages (nadir) with a resolution of 12.5 or occasionally 25 m/px served to localise ILDs in the equatorial region.
These ILDs were then described in detail through HRSC and MOC images (Sect. 3.1.2). In addition, HiRISE-images (Sect. 3.1.4) were used later on. MOC images were downloaded from the Malin Space Science Systems[18] with a spatial resolution of ~2.8 m/px (Table 8). HiRISE-images were downloaded from the NASA JPL site[19] with a resolution of 0.25 m/px and projected to obtain detailed information about surface morphology.
Image mosaics were generated to visualise the context of examination of HRSC, THEMIS and MOC image data (Table 8) under DLR VICAR software.

Relative Albedo

The albedo is important in describing the surface state of ILDs as it demonstrates the reflected fraction of the total light or other radiation falling on a non-luminous body. The Lambert albedo is low (0) in a totally black surface and high (1) in a perfect reflector and dark body [*Ridpath*, 2003], permitting ILDs to be classified by their reflexion behaviour. In general, it is equal to the amount of light reflected divided by the amount of light received and thus is the relation between radiation and reflexion ranging from 0-1. Moreover, albedo is controlled by the wavelength of light under examination.

[18] http://www.msss.com
[19] http://hirise.lpl.arizona.edu

In this case, what was determined was not the albedo but relative gray-scale brightness so that ILDs could be classified as low, intermediate and high albedo, supported by additional parameters. The relative albedo is listed in the table together with ILD parameters (Table 23), inner regions not being considered in the table but in the ILD description such as for characterisation of different morphological units.
Besides, albedo features have to be treated with caution, as some features that are markedly darker or brighter than their surroundings do not necessarily correspond to a topographical or geological feature, and shadows stimulate low-albedo features.

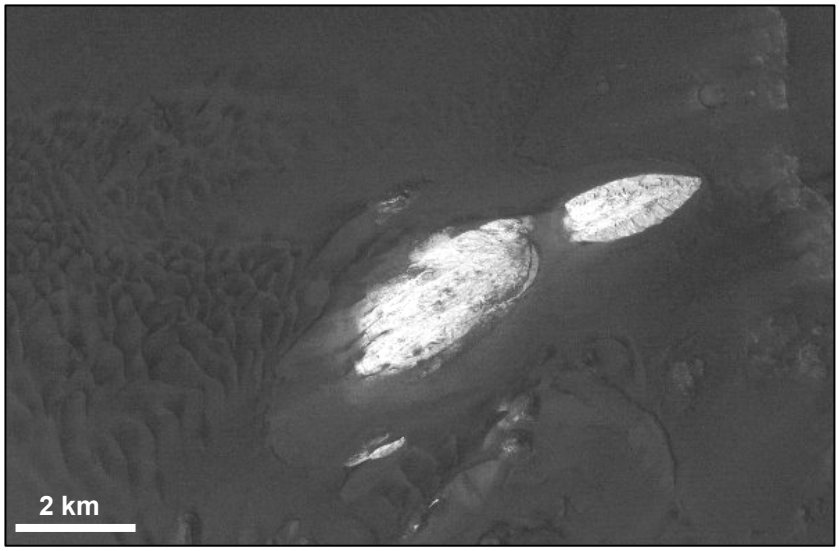


**Figure 16:** HRSC nadir image (orbit h2178_000; 7.4°S/312.9°E) illustrates the relative albedo of an ILD and its surrounding. The ILD shows the highest albedo, whereas dark dunes and the chasma floor feature a much lower albedo. Dark patches on the ILD surface mostly correspond to dark aeolian material as well.

Consolidation of materials

Consolidation is an important source of information about a material and the type of weathering it experienced. In ILDs, comparable materials consolidation may indicate comparable material and climatic conditions, whereas different material consolidation may point to differences in type of weathering (Sect. 2.2.1, 2.3.1), base material, age (Sect. 2.3.4, 2.4.3), or regional (climatic) conditions (Sect. 2.2).
The resolution of HiRISE (Sect. 3.1.4) is ten times higher (0.25 m/px) than that of MOC (Sect. 3.1.3), HiRISE being the camera with the highest spatial resolution that is now orbiting Mars (Table 2, 8). Its images reveal the consolidation of materials on ILDs surface (possible jointing and fracturing) as well as the deposition of boulders and talus derived from broken material.
THEMIS BT (Sect. 3.1.6) and TES TI (Sect. 3.1.5) were combined with image data to characterise those thermophysical properties of the material that are associated with consolidation (Table 8, Sect. 3.2.2).

### 3.2.2 Spectroscopy

There are several methods and techniques of obtaining information about the composition, structure and texture of planetary surfaces, including spectrophotometry [*Jaumann*, 1989]. These methods are based on the detection of emitted and reflected electromagnetic radiation. Data acquisition is strongly related to the sensitivity of the detectors. Spectrophotometry is an essential tool for the geochemical and mineralogical exploration of solid planetary surfaces [*Karr*, 1975]. Spectrophotometry measures spectral reflectance [*Slater*, 1983], which is the fraction of incident and reflected light in the visible and near-infrared spectral range.
Laboratory experiments on chemically and mineralogically well-known rock and mineral samples permit comparing and interpreting spectra taken by remote sensing techniques. In laboratory measurements, physical factors (e.g. temperature, pressure and weathering) must be considered. To interprete a spectrum, it is necessary to understand the optical absorption bands of rocks and minerals. Thus, ratio spectra are useful to enhance spectral signatures (absorptions) in the target spectrum and to allow for atmospheric conditions during the observation [*Mustard et al.*, 2005]. In this case, the target spectrum is divided by a region nearby.
Minerals that occur on Mars and are somehow associated with ILDs will be described by their spectral properties. These minerals are olivine, pyroxene, feldspar, haematite, phyllosilicates, and sulphates. The data that were used in the spectral interpretation will be described subsequently. Of particular interest are the sulphates and haematite since these minerals are directly associated with ILDs [e.g. *Gendrin et al. 2005*; *Glotch and Rodgers*, 2007]. Both minerals groups and requirements for their formation are listed in detail.

Olivine $(Mg, Fe)_2[SiO_4]$
Olivine and pyroxene are widely distributed over the Martian surface [*Mustard et al.*, 2005]. They are detectable by spectrometers because visible/near-infrared (NIR) reflectance measurements are sensitive to crystal-field transition in iron-bearing mafic minerals (Sect. 3.1.7, 3.1.8, Table 2, Table 8). As their origin is associated with magmatic processes, they also form an important source of information about potential secondary minerals.
Olivine is a mixed crystal alignment between forsterite ($Mg_2SiO_4$) and fayalite ($Fe_2SiO_4$). In the common terrestrial rock-forming olivine, the forsteritic component dominates. Olivine is abundant in meteorites, lunar rocks, and terrestrial mafic and ultramafic rocks [*Matthes*, 2001].

The olivine spectrum shows characteristic absorptions centred near 1 µm (Fig. 17) resulting from crystal-field transitions in the $Fe^{2+}$ ions in the fayalite molecule fraction [*Karr*, 1975]. Increasing iron content and grain size [*Mustard et al.*, 2005] causes an increase in band depth and a shift to longer wavelengths towards an inflection near 1.3 µm. The 1.03-1.05 µm absorption band is characteristic for forsteritic olivines; there are but several other minerals such as calcium pyroxene, that feature an absorption band in that range, but these minerals do have additional characteristic bands at other

wavelengths.
On certain Martian surfaces, a strong broad absorption between 0.8 and 1.5 µm has been observed [*Mustard et al.*, 2005] which might be due to increased iron content or grain size.

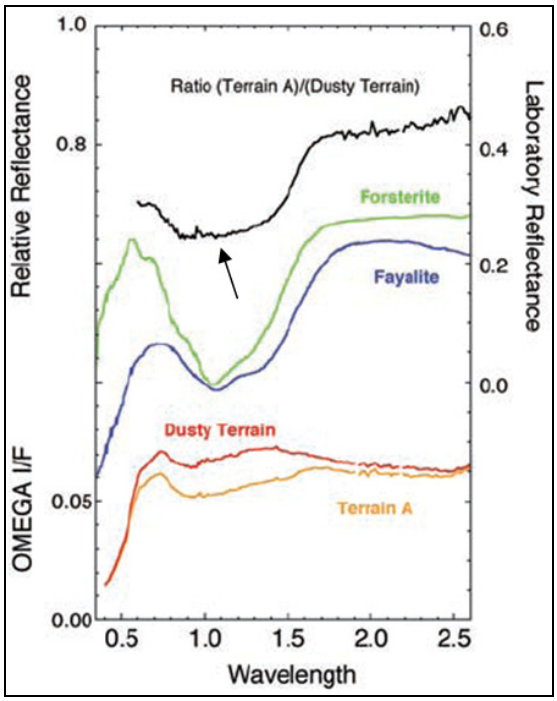


**Figure 17:** Olivine spectra by *Mustard et al.* (2005). OMEGA I/F (incident solar flux) atmospherically corrected spectra are shown with the target spectrum (Terrain A, *top*) and a nearby spectrally neutral region (Dusty Terrain, *below*), laboratory spectra of fayalitic and forsteritic olivine *(centre)*, and ratio of Terrain A/ Dusty Terrain *(bottom)* emphasising absorption bands that are characteristic for olivine.

## Pyroxene $X^{[8]}X^{[6]}[Z_2O_6]$[20]

Pyroxenes are abundant in terrestrial rocks, meteorites, and asteroids as well as on Mars [*Karr*, 1975], where high calcium pyroxene (HCP) is distinguished [*Mustard et al.*, 2005], a clinopyroxene comparable to diopside ($CaMg[Si_2O_6]$), and low-calcium pyroxene (LCP) an orthopyroxene corresponding to the enstatite ($Mg_2[Si_2O_6]$) - ferrosilite ($Fe_2[Si_2O_6]$) mixed crystal alignment [*Matthes*, 2001].

Pyroxenes show the best-defined absorptions bands of all rock-forming silicates. The first band at 0.9 µm is deep and narrow; the second is at 1.8-2.0 µm (Fig. 18). These absorption bands result from crystal-field transitions in $Fe^{2+}$ and shift to longer wavelengths as the increasing calcium, and iron content increases [*Karr*, 1975], which may be the case on the Martian surface (Fig. 18).

[20] positions of $X^{[8]}$ can be occupied mainly by $Na^+$, $Ca^{2+}$, $Fe^{2+}$, $Mg^{2+}$, $Mn^{2+}$; $Y^{[6]}$ by $Fe^{2+}$, $Mg^{2+}$, $Mn^{2+}$, $Zn^{2+}$, $Fe^{3+}$, $Al^{3+}$, $Cr^{3+}$, $V^{3+}$, $Ti^{4+}$; and $Z^{[4]}$ by $Si^{4+}$, $Al^{3+}$ [*Matthes*, 2001].

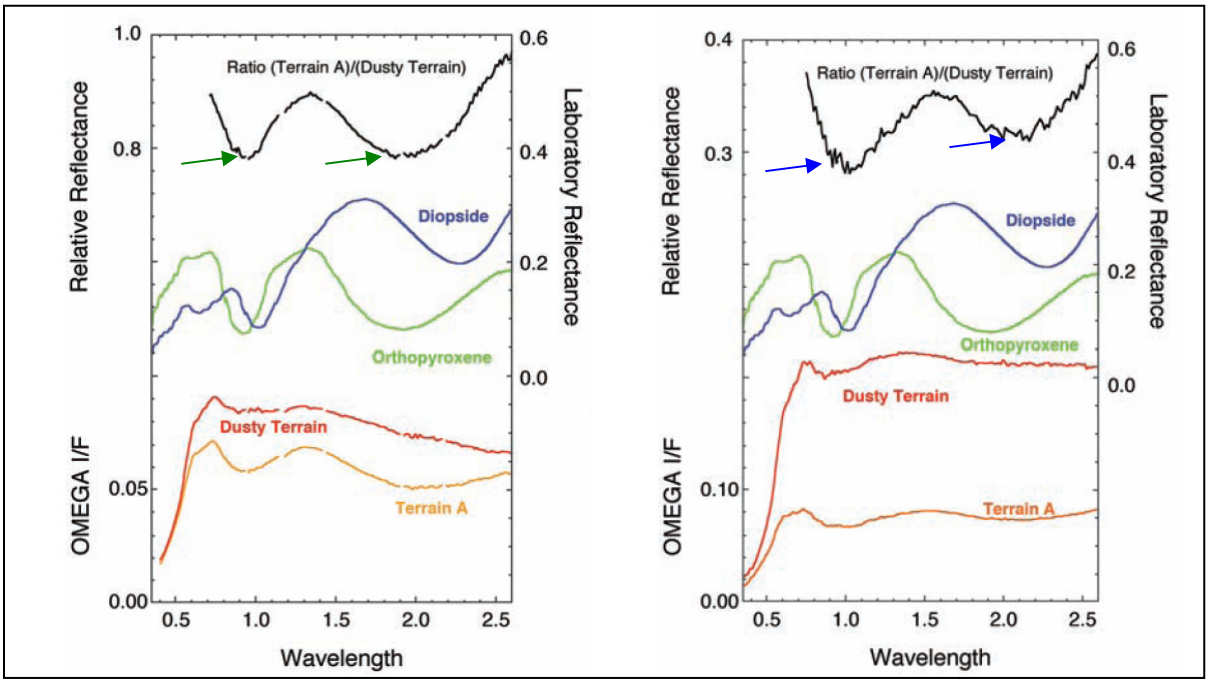


**Figure 18:** Pyroxene spectra from *Mustard et al.* (2005). OMEGA I/F atmospherically corrected spectra with target spectrum (Terrain A, *bottom*) and a nearby neutral region (Dusty Terrain, *bottom*), laboratory spectra of HCP (diopside, *centre*) and LCP (enstatite, *centre*), and ratio of Terrain A/ Dusty Terrain *(top)*. Spectral ratio emphasises absorptions (arrows) near 0.9 µm and 1.9 µm corresponding to LCP *(left)* and *(right)* spectral ratio indicating absorptions near 1.05 µm and 2.3 µm indicating HCP.

## Feldspars

Feldspars are a ternary mixing system of orthoclase [$KAlSi_3O_8$], albite [$NaAlSi_3O_8$] and anorthite [$CaAlSi_2O_8$]. Minerals ranging between the mixed crystal alignment of orthoclase and albite are called alkali feldspars, while those between albite and anorthite are plagioclases [*Matthes*, 2001]. Feldspars are abundant on Earth, constituting about 60% of the continental crust. On Mars, plagioclase was detected by TES [*Bandfield*, 2000; *Glotch and Christensen*, 2005; Table 8], not by OMEGA or CRISM (Sect. 3.1.7, 3.1.8), because of the different wavelength range and lower sensitivity (Table 8). TES spectral range extends to the thermal infrared to 5.8-50 µm (Table 8) and therefore is able to identify feldspar that features absorption bands around 10 and 25 µm.

Besides water bands at 1.4 µm and 1.9 µm caused by trapped and/or absorbed water, feldspars also show absorptions resulting from trace amounts of $Fe^{2+}$ and $Fe^{3+}$ [*Karr*, 1975]. Plagioclases feature absorption bands between 1.1 and 1.3 µm due to $Fe^{2+}$, in addition, a weak $Fe^{3+}$ band may show at 0.86-µm. The extent of the $Fe^{2+}$ band varies depending on the crystal structure and the albite-anorthite ratio.
Conversely, alkali feldspars show no detectable $Fe^{2+}$ absorption feature but an $Fe^{3+}$ absorption at 0.86 µm and another sharp edged one at 0.5 µm.

Hydrated minerals like sulphates and phyllosilicates have been detected on Mars by OMEGA/MEX [*Gendrin et al.*, 2005; *Poulet et al.*, 2005], direct records of past aqueous activity (e.g. Table 8, Sect. 3.1.7). These minerals provide information about the influence of environmental processes on the abundance and permanence of water and the

importance of chemical alteration processes. Alteration products are supposed to have been formed by various formation processes occurring during distinct climatic episodes.
Hydrated minerals are identified by their characteristic 1.9 µm band [*Gendrin et al.*, 2005; *Poulet et al.*, 2005]. They contain OH ions and $H_2O$ molecules, which cause vibrational absorption signatures.

Phyllosilicates

Phyllosilicates occur in the Earth's crust besides quartz and feldspar. They are present in weathered sediments and altered magmatic rocks, i.e. result from weathered silica such as feldspars [*Matthes*, 2001].
On Mars, clay minerals have been detected (Fig. 19), which are mainly associated with Noachian outcrops indicating an active hydrological system earlier on [*Poulet et al.*, 2005].

Phyllosilicates exhibit absorptions resulting from OH at 2.2-2.4 µm and $H_2O$ around 1.9 µm as well as from $Fe^{2+}$ and $Fe^{3+}$ [*Karr*, 1975].
Here, only clays will be considered as they occur on the Martian surface [*Poulet et al.* 2005]. The 1.9 µm band is present in clays, especially in water-bearing clays which also show weak bands near 1.15 µm and 0.95 µm, overlapping possible iron-induced bands. However, in the presence of water the 1.9-µm band in clays is ten times deeper than the 0.95 and 1.15 µm bands [*Karr*, 1975].
On Mars, clay minerals were found whose spectral signatures resemble those of nontronite [$Na_{0.3}Fe^{3+}{}_2(Si, Al)_4O_{10}(OH)_2.n(H_2O)$][21], chamosite [$Fe_3Mg_{1.5}AlFe_{0.5}Si_3AlO_{12}(OH)_6$] and montmorillonite [$Na_{0.2}Ca_{0.1}Al_2Si_4O_{10}(OH)_2(H_2O)_{10}$] were found [*Poulet et al.*, 2005]. Metal-OH vibrations were observed in the 2.2-2.4 µm range in addition to the water band near 1.9 µm (Fig. 19).
*Poulet et al.* (2005] specifically identified nontronite by its 1.41, 2.29, and 2.40 µm bands that are characteristic for a Fe-rich smectite (Fig. 19). Chamosite shows absorptions at 1.41 and 2.35 µm, and montmorillonite displays bands at 1.41, 2.21, and 2.35 µm, which matches phyllosilicates of that composition.

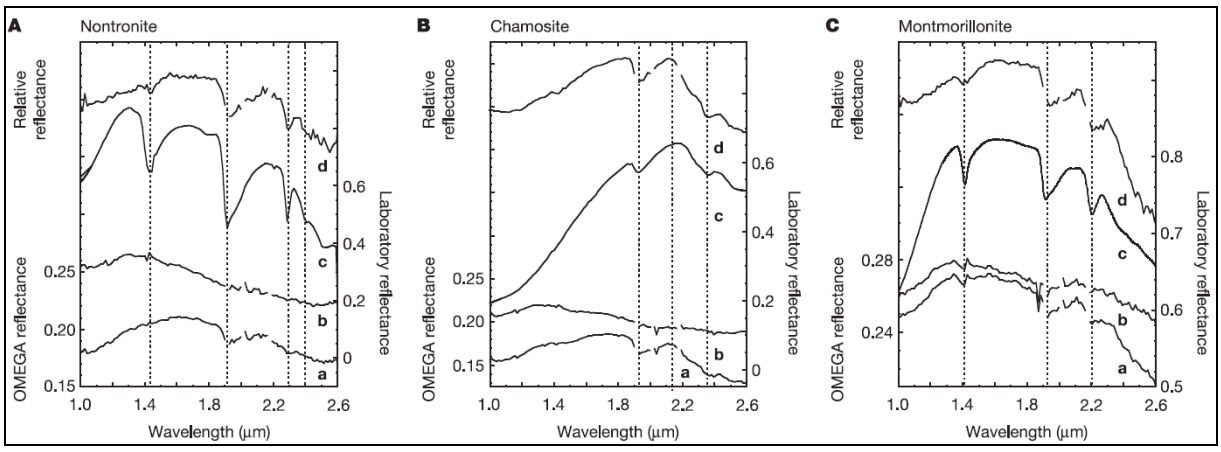


**Figure 19:** Phyllosilicate spectra from *Poulet et al.* (2005). I/F atmospherically corrected OMEGA-spectra (a, b) for nontronite (A), chamosite (B) and montmorillonite (C). a: phyllosilicate spectrum, b: reference spectrum (nearby region of a), c: laboratory spectrum, and d: spectral ratio of a/b to emphasise absorption

[21] http://www.webmineral.com

bands.

Sulphates [$X_nSO_4*nH_2O$]

On Earth, sulphates primarily form thick beds produced by the evaporation of seawater. Hydrothermal or diagenetic alterations caused by acidic groundwater in rocks may also form sulphates.

On Mars, sulphates were found in ILDs (Fig. 20, Sect. 1, 2.4.3) located in certain chasmata of Valles Marineris and chaotic terrains [e.g. *Gendrin et al.*, 2005]. As they were identified as water-bearing by their characteristic NIR bands they will be considered here. Among them are monohydrated sulphates (gypsum $CaSO_4*2H_2O$, kieserite $MgSO_4*H_2O$) and polyhydrated sulphates (in this case epsomite $MgSO_4*7H_2O$ and hexahydrite $MgSO_4*6H_2O$; *Gendrin et al.*, 2005). Of these, gypsum and epsomite

Gypsum has many settings of formation but however it forms at low temperatures and positive oxidation potential [*Rösler*, 1984]:

- Huge amounts are formed in salt lakes and barres by evaporation in assemblages with carbonate, halite, and other salts;
- in deserts it precipitates in sediments and soils as nodules, concretions, cement of sands and joint-filling material,
- in a hydrothermal milieu it is rarer but it forms more often by sulphide oxidation in the oxidation zone of ore deposits;
- the majority is formed by a conversion of anhydrite into gypsum which takes place at the surface by water absorption during weathering in a humid climate ($Ca[SO_4] + 2H_2O \rightarrow Ca[SO_4] * 2H_2O$).

The formation of kieserite is restricted to certain thermodynamic conditions [*Vaniman et al.*, 2004] and under the presence of water it is easily converted to PHS (i.e. hexahydrite and epsomite). These minerals are not transformed back to kieserite. Kieserite therefore is likely not formed in deposits that were exposed to water and desiccation for multiple times [*Gendrin et al.*, 2005].

According to Warren (2006), kieserite is formed by:

1) precipitation in an aqueous system at the surface
2) dehydration of hydrated material via lithostatic pressure at depth
3) alteration of minerals during subsurface circulation

It does not form at ambient temperatures on Earth except in hot desert regions, as it requires temperatures of 30-50°C for its formation [*Mangold et al.*, 2008].

Epsomite forms secondarily by oxidation of iron sulphides or by evaporation in salt lakes on Earth. In addition, it transforms from kieserite by water absorption. It often occurs as a weathering product of kieserite accompanied by hexahydrite and other $MgSO_4$-hydrates [*Rösler*, 1984].

Based on laboratory investigations [*Vaniman et al.*, 2004], PHS and kieserite form under

different conditions. Moreover, under Martian conditions dehydration of PHS rather form an amorphous PHS than kieserite. Furthermore, as crystallisation of amorphous PHS to kieserite is a long-term process, it is more likely that PHS form from rehydration of kieserite as a result of meteoric water absorption.

Hydrated minerals show the characteristical 1.9 µm band corresponding to water. However, kieserite is identified by bands close to 1.6, 2.1, and 2.4 µm, PHS by spectral feature close to 1.4, 1.9, and 2.4 µm and gypsum by the 1.4, 1.75, 1.9, and 2.2 µm absorption bands [*Gendrin et al.*, 2005].

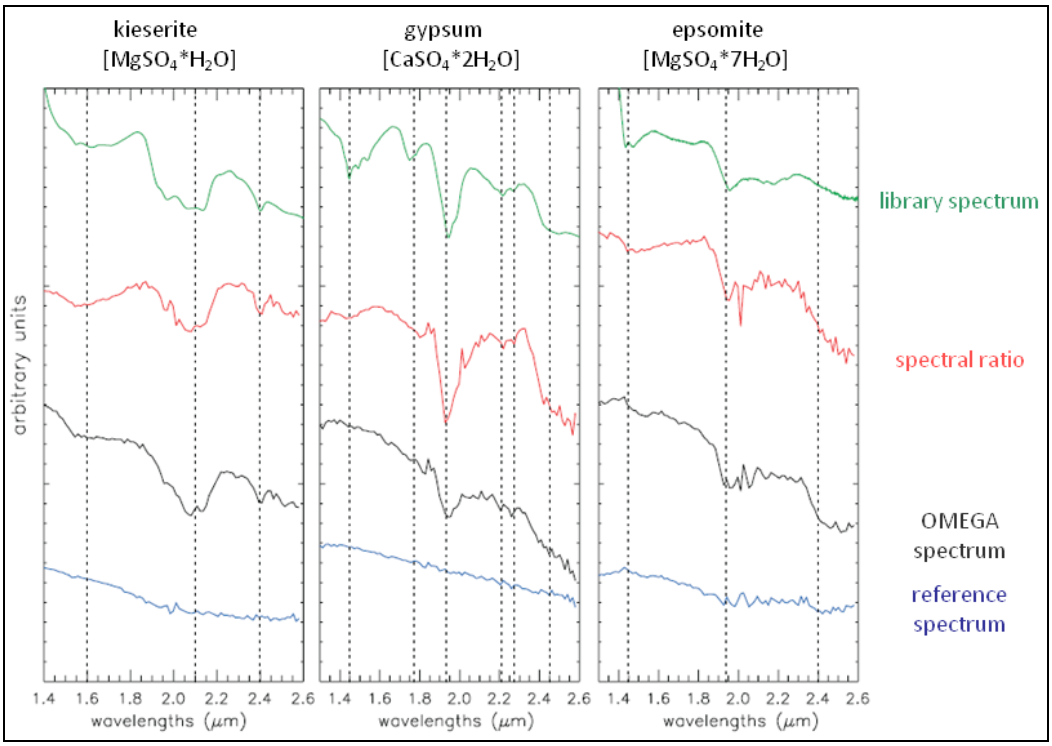


**Figure 20:** Sulphate spectra from *Gendrin et al.* (2005). I/F atmospherically corrected spectra (blue, black) and spectral ratio in comparison with library spectrum.

Absorptions mainly result from different combinations and overtones of OH and $H_2O$. On Earth, the amount of gypsum is very high compared to kieserite. The possibility that mafic crsut alterations may have caused higher Fe and Mg contents in Martian than in terrestrial brines might explain the formation of sulphates in addition to carbonates and other salts.

Haematite [$Fe_2O_3$]

The haematite concretions known from Earth are usually formed by subsurface precipitation in flowing water. On Mars, the exploration rover Opportunity also discovered marble-shaped pebbles called „blueberries“ [*Catling*, 2004].

Haematite is a mineral that in most cases requires water for its formation, but it can also result from a dry, thermal oxidation process. On Mars, it is closely connected to ILDs and sulphates [e.g. *Gendrin et al.*, 2005; *Glotch and Christensen*, 2005]. It either occurs as spherules on surface layers and in shallow depressions. It is assumed that water was involved in its formation in Meridiani Planum [*Hynek et al.*, 2002]. Therefore, the presence of haematite indicates that conditions on Mars were wetter and warmer when

the haematite originated.
There are many explanations of how the haematite in Meridiani Planum was formed [*Chan et al.*, 2004]:

- Precipitation in large lakes or hot springs (during ancient Tharsis volcanism),
- residue when water leached away other minerals,
- chemical alteration of volcanic ash deposits.

On Earth, it has a broad area of formation, whereupon the focus is at intermediate temperatures [*Rösler*, 1984]. It occurs:

- Finely dispersed and reddish in the weathering crust where it is primary formed by dehydration of limonite; it is enriched in oxidation zones of ore deposits,
- as primary hydrothermal formation in
  - in dyke deposits,
  - in volcanic craters and their surrounding (especially submarine),
- by dehydration and oxidation of sedimentary limonitic and hydro haematitic ores due to diagenesis and metamorphosis,
- by oxidation resulting from martitisation of magnetite; in clastic sediments as it is chemically resistant.

Haematite features strong and narrow absorption bands at 0.85 µm (Fig. 21) and a broad saucer-shaped band at 1.0 µm and 2.5 µm caused by $Fe^{3+}$ iron charge transfer [*Karr*, 1975]

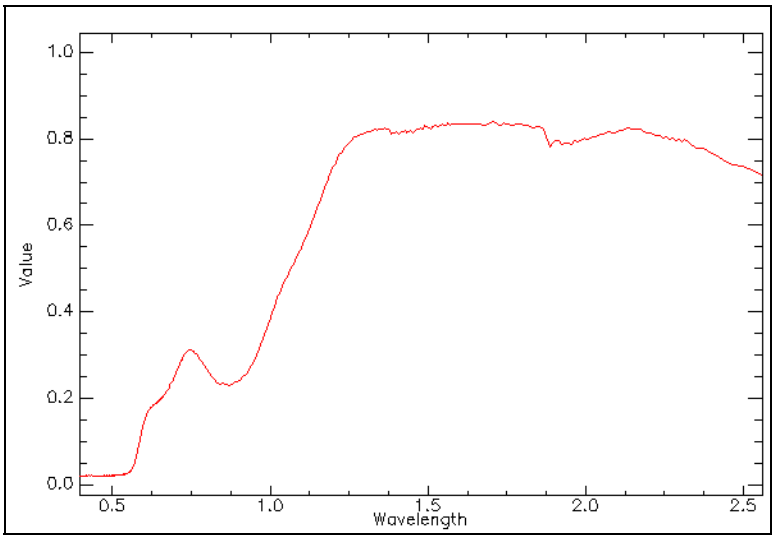


**Figure 21:** Haematite laboratory spectra. In the visible to near-infrared band, haematite features characteristic absorptions (arrows) at ~0.9 µm and between 1-2.5 µm. Spectra reproduced from the ENVI spectral library.

Spectral interpretation was based on HRSC false colour images, THEMIS nighttime infrared images and deduced brightness-temperature data, TES TI readings, and mineralogical information from OMEGA and CRISM.

Colour of materials
HRSC features four colour channels (Sect. 3.1.1, Fig. 22, 15) for multispectral observations

of the Martian surface. The colour channels reveal compositional discrepancies on the surface and in the atmosphere [*Jaumann et al.*, 2007]. Basically, these heterogeneities result from oxidised, unoxidised materials and ice. Therefore, they are useful to distinguish between spectral differences especially between different layers within an ILD and its surroundings which indicate different mineralogies (Fig. 22). For small-scale analysis, HiRISE colour images (Sect. 3.1.4, Table 8) were examined.

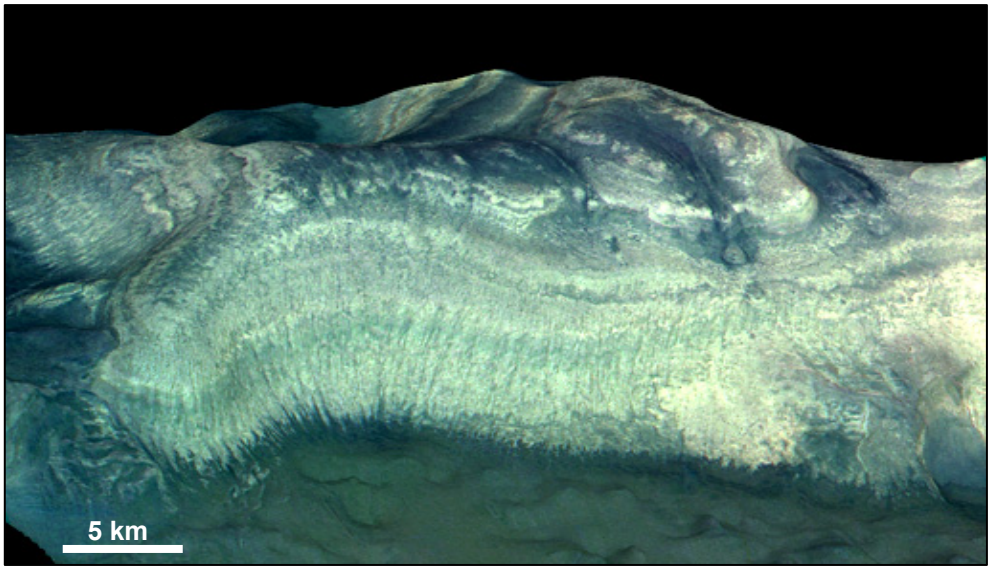


**Figure 22:** HRSC false colour in perspective view. Minerals appear in different tints within the layered sequence. There is dark (bluish) aeolian material covering parts of the ILD (orbit h2211_0000; 7.1°S/312°E).

Thermal Inertia (TI)

TES TI (Sect. 3.1.5, Table 8) data were used because they contribute to a better understanding of the consolidation of materials especially within layers. Thermal Inertia $I$ reflects the physical properties of the surface and is therefore affected by material properties like density $\rho$, heat capacity $c$, and thermal conductivity $k$ (Eq. I). SI[22] units of TI are expressed as [J/ m²*√s*K].

$$I = \sqrt{k\rho c} \qquad \text{(I)}$$

It reflects a combination of particle size, rock abundance, bedrock outcropping the degree of induration. Unlike an optically thick deposit, a thermally thick deposit only affects the surface temperature [*Pelkey et al.*, 2001]. The temperature of an ideally flat, uniform, and homogeneous surface throughout the day depends primarily on the diurnal skin depth $\delta$ of the surface material.

$$\delta = \frac{I}{\rho C}\sqrt{\frac{p}{\pi}} = \sqrt{\frac{k\ p}{\rho C\ \pi}}, \qquad \text{(II)}$$

[22] SI: ***S**ystème **i**nternational d'unités* (Internationales Einheitensystem)

Here, thermal inertia is $I$, bulk density $\rho$, thermal conductivity $k$, and the length of a day $p$.

A thermally thick deposit, therefore, must have a minimum thickness of one diurnal skin depth [*Jakosky*, 1979]. Thermal thickness and diurnal skin depth in turn, are gouverned by physical properties. For air fall dust, diurnal skin depth is ~1 cm [*Pelkey et al.*, 2001]. A thermally intermediate deposit must be at least one diurnal skin depth thick to affect the surface temperature. The surface is not affected by thermally thin deposits (thickness << diurnal skin depth; airborne dust thickness < 1-3 mm).

The thermal skin depth [*Jakosky*, 1986] of loose sandy material which covers a rock at a thickness of less than ~7.5 cm shows a TI pointing to the underlying material [*Edgett and Christensen*, 1991]. Otherwise, TI reflects the loose surface material.

Nighttime surface temperatures are used to observe the TI of the material relative to its surroundings. A high TI indicates a more consolidated, coarser material corresponding to bright regions that have higher surface temperatures and are able to keep the heat for a much longer time [*Jakosky et al.*, 2000]. THEMIS brightness-temperature (BT; cf. Sect. 3.1.4, Table 8) is closely related to TI. Dark regions show lower surface temperatures and TI as they often consist of unconsolidated, dusty, fine-grained material that cools out much faster during nighttime. According to *Putzig et al.* (2005), surfaces can be globally classified as rock or loose material by their albedo and TI. A TI of >386 SI indicates rocks, bedrock, duricrusts and polar ice whereas a TI of 140-386 SI indicates sand, rock, bedrock and some duricrusts. However, this classification is large-scale, and it will be assessed whether ILDs fit into these groups.

Bolometric TES data were downloaded from the Arizona State University (ASU) TES-site[23] and TI was extracted. Data selection was based on the following criteria: Local time was defined as nighttime (6.00 p.m.-6.00 a.m.), emission angle was set ≤ 3, quality bolometric inertia ranking = 1, and quality bolometric lamp anomaly was set = 1. The translation of TES data into ArcGIS [*Saiger*, 2008] permits exact TI measurements (Fig. 23). For improved demonstration, images were resampled into cubic convolution. Due to the low spatial resolution of the instrument (3 km/pix, Table 8), it is not only appropriate for describing small-scale features.

The mean TI values of each ILD and its surroundings were determined and listed in the ILD parameter tables together with the respective standard deviation (e.g. Ø350 SI±55). Based on its mean TI, each ILD was classified as low (304-368 SI), intermediate (379-424 SI), and high (428-498 SI) TI using univariate statistics. Combined with other datasets, TI is appropriate for characterising surface materials and deducing formation scenarios.

[23] http://tes.asu.edu

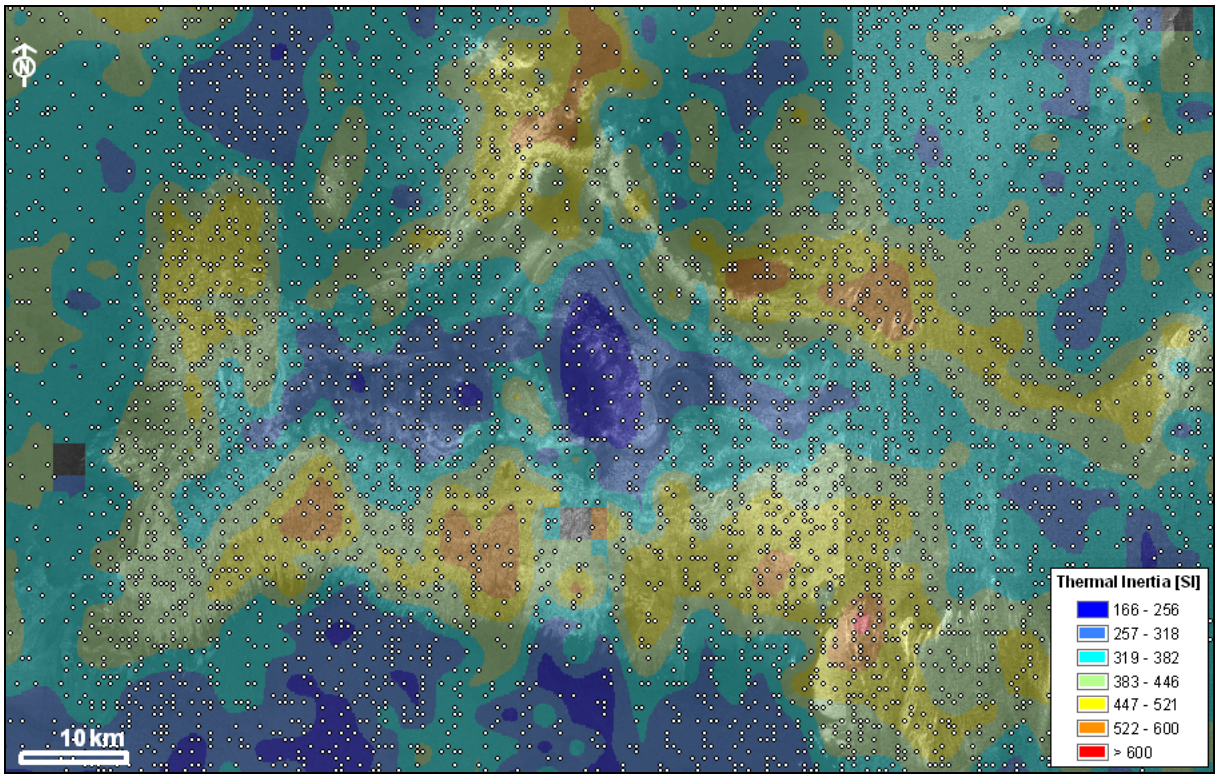


**Figure 23:** TES TI map. Values are resampled with cubic convolution for improved demonstration. Dots correspond to single TES data points that were used to determine the TI of ILDs and their surroundings. High TI is corresponds to yellow to red colours indicating more consolidated material than shown in bluish colours (7.1°S/312°E).

### Brightness Temperature (BT)

In order to identify material differences THEMIS data (Sect. 3.1.6, Table 8) were used to obtain information about the consolidation of ILD material. Besides, these data may served to detect differences in layering and thus to characterise ILDs. Nighttime infrared images with a spatial resolution of 100 m/ px were downloaded from the ASU THEMIS site[24]. BT showed the surface temperatures of ILDs relative to their surroundings (Sect. 3.1.6; Fig. 24).

THEMIS daytime images display temperature differences between sunlit (warm, bright) and shaded (cold, dark) slopes, contrasting with nighttime images in which the effects of heat and shade on the slopes are no longer present. Rocky materials retain their heat at night and stay warm, whereas fine-grained dust and sand cools off more rapidly. A small amount of atmospheric dust is seen by THEMIS, but surface dust with a thickness of no more than~100µm will obscure any underlying thermal IR signatures. Contrary to TES (Sect. 3.1.5), it is an imaging spectrometer and therefore provides raster data besides ASCII data (Table 8).

[24] http://themis-data.asu.edu/

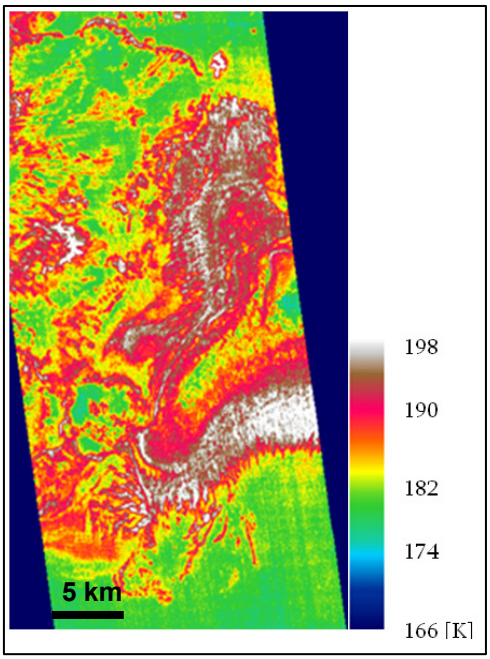


**Figure 24:** THEMIS BT map. Differences in surface temperature derived from brightness-temperatures are colour-coded. ILD surface shows medium (green: 182 K) to high (white: 198 K) temperatures relative to its surroundings indicating higher consolidated material in regions of higher temperatures (orbit I01706003RDR; 7.3°S/310.4°E). More fine-grained material like dust or sand cools more rapidly at night indicating lower surface temperatures at night contrary to rocky materials.

OMEGA

OMEGA analyses of *Gendrin et al.* (2005), *Mangold et al.* (2007) and *NoeDobrea et al.* (2008) were used to get mineralogical information of the ILDs.

CRISM

In addition, CRISM analyses (Table 8, Sect. 3.1.8) were used in a collaboration framework. The data were processed and analysed by Leah Roach of Brown University. The aim was to look for differences in mineralogy between ILDs to find out whether specific mineralogies are ascribed to defined morphologies to deduce possible correlation between ILDs. Therefore, HiRISE (Table 8, Sect. 3.1.4) and CRISM were used in combination. Unfortunately, not all ILDs are covered by CRISM (Aureum 1, Ganges 3+5, Iani 1). Especially for these smaller ILDs CRISM data are more useful as pointing is more precise due to the high spatial resolution and mineral exposures can be pulled together with morphology.

ILDs are named spectrally neutral when they do not show absorption bands in the VNIR (visible-near infrared), in which OMEGA and CRISM are able to identify absorptions (Table 8). These minerals do not show iron or hydration features, carbonates or nitrates in the required spectral range (Table 8; Sect. 3.1.8). Thus, spectrally neutral minerals might be other sulphates (e.g. anhydrite), halite or sylvite, or even siliceous minerals (e.g. plagioclase) that show no absorptions in the VNIR.

### 3.2.3 Interpretation of elevation-derived data

For 3D interpretation HRSC DTMs (digital terrain models, Sect. 3.1.1, Table 8) and a MOLA DEM (digital elevation model, Sect. 3.1.2, Table 8) processed at the DLR were used. DTMs consist of high-level HRSC data that are useful to describe the Martian topography in detail because every point on the surface is mapped from various perspectives. From this information, elevation data are computed using all stereo channels (Fig. 25, 15, Sect. 3.1.1). These data are used to describe ILD elevation, thickness, slope, and layering geometry.
Anaglyphs views were generated to obtain a more precise impression of the stratigraphic relationships between units within ILDs. Moreover, profiles were developed from HRSC and MOLA data to visualise the morphology and surroundings of ILDs.

Profiles
Profiles were created to demonstrate the ILD morphologies and internal structures, using both HRSC DTMs (Table 8) and MOLA DEMs.
A line from A to A' covering the body as well as top of the ILD was drawn in ArcGIS using HRSC and MOLA topography which specifies distance (x-axis) versus topography (y-axis; Fig. 25). Subsequently, the data were exported to MS EXCEL to prepare the cross-section (Fig. 25).
Using HRSC DTMs, the y (topography) axis attains an accuracy that is comparable to the HRSC-nadir resolution [*Gwinner et al.*, 2005; *Jaumann et al.*, 2007] that is ±12.5-50 m/px (Table 8, Sect. 3) in the best case. The x (distance) axis accuracy is ±50-150 m/px. In a MOLA DEM, the topographic accuracy is ±2 m/px and the sampling distance is ±463 m/px at best (Table 8, Sect. 3.1.2).
For most of the targets, HRSC DTMs are available, which were duly used. DTMs are especially useful for local, small-scale measurements of elevation, thickness, layer geometry and slope because of their high spatial and vertical resolution.
MOLA DEMs were used for regional measurements to demonstrate the relationship between ILDs and their surroundings such as plateau rims, for overviews and longitudinal profiles, and if no DTMs are available.
From the profiles and terrain models, the minimum and maximum elevations of ILDs were derived. These elevation ranges correspond to the minimum and maximum elevations at which ILD of the same morphology were observed.

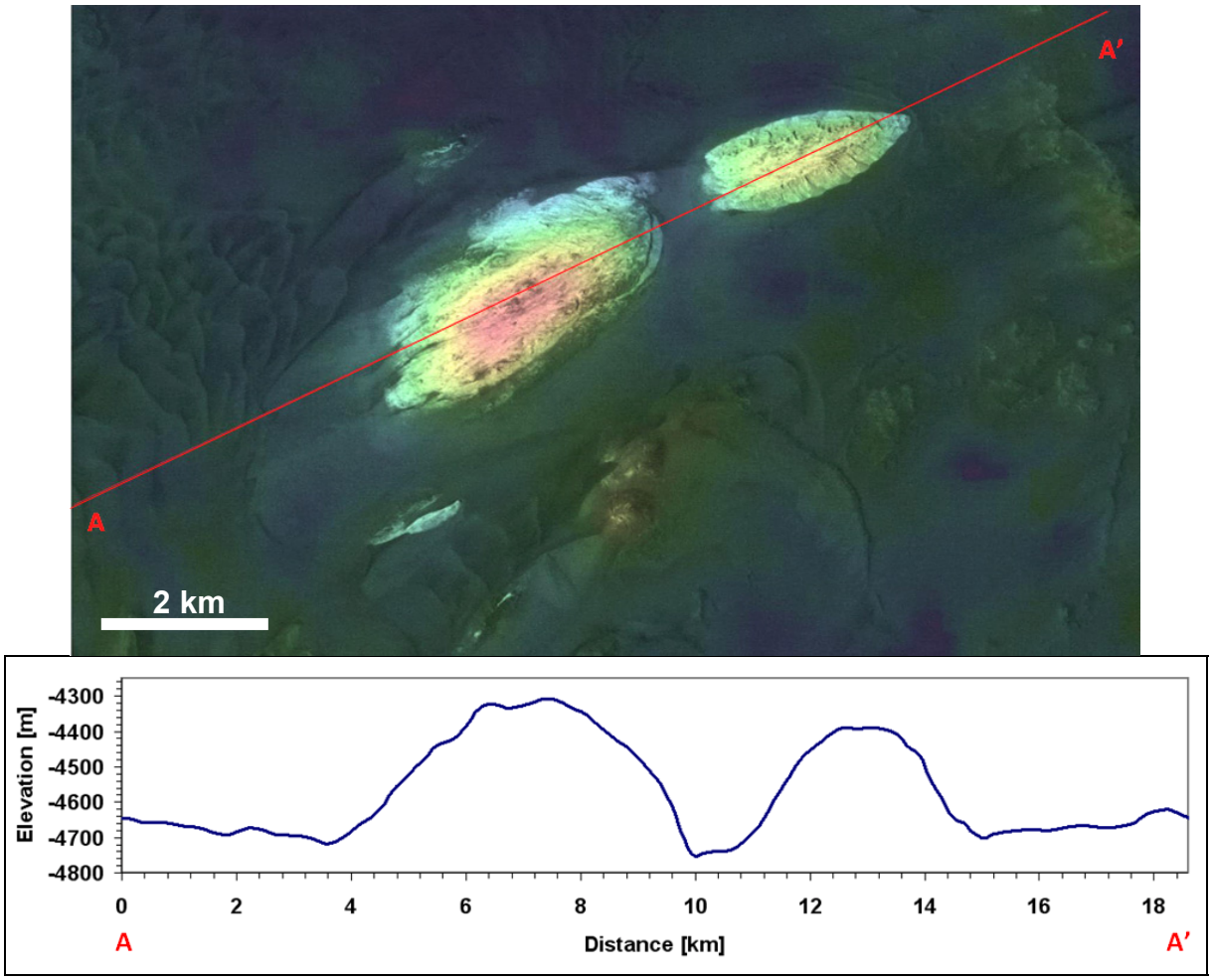


**Figure 25:** HRSC-DTM profile. *(top)* Location of profile A-A' covering the ILD (h2145_0000; 7.4°S/312.9°E). *(bottom)* The x axis, corresponding to distance, has an accuracy of ±0.05 km. The y axis, corresponding to topography, is correct to ±12.5 m.

## Layering geometry

Using the Pangaea Scientific Orion™[25] structural analysis software, the strike and dip of layers was defined to obtain an impression of the internal structure of ILDs and deduce possible formation hypotheses (Sect. 1) as well as to discuss their association with regional tectonics. For this purpose, HRSC orthoimages and corresponding DTMs were used. These measurements were applied to ILDs that show layering that is traceable throughout the whole ILD, providing that the ILD in question was covered by DTMs with a spatial resolution of less than 75 m.

Layering geometry measurements were performed to confirm a sedimentary or possible volcanic origin due to strike and dip of the layers. Sedimentary, waterlain deposits are horizontally layered unless they experienced post-depositional tilting whereas volcanic deposits are more likely inclined [*Hauber et al.*, 2005].

First, a plane comprising at least three points had to be defined. For this purpose, points were manually sampled from the nadir image along the exposed part of the layer. Orion software then computed the horizontal and vertical coordinates of the points on the layers

[25] http://www.pangaeasci.com/_orion.htm

[*Fueten et al.*, 2005]. It uses the variations in point elevation to compute the best-fit plane by multilinear regression. The regression equation is defined as

$$Z = a + bX + cY \tag{III}$$

where $Z$ is the elevation, a, b, and c are the regression coefficients, $X$ is the easting and $Y$ the northing [*Fueten et al.*, 2005]. The coefficients were calculated by standard regression. The attitude of the plane (strike $S$ and dip $D$) was related to the regression coefficients by

$$S = \arctan(\frac{b}{c}) + \frac{\pi}{2} \tag{IV}$$

and

$$D = \arctan\left(\frac{1}{\sqrt{b^2 + c^2}}\right) \tag{V}$$

For further information, see *Fueten et al.* (2005).
Elevations and x and y coordinates were captured along the plane to calculate the strike and dip relative to horizontal deviation. For each of these layers, an error factor was computed, and measurements were repeated to improve the accuracy. Then, the root mean square (RMS) error was calculated.
Certainly, measurements from orbit cannot be as accurate as from ground truth, for instance often there is uncertainty in whether layers or slope are measured. To minimise slope effects, the dip measurements have to be compared to slope maps of the respective region. Unfortunately, these uncertainties cannot be ruled out completely. Layering is stated sub-horizontal in case dip angles are < 10° due to measurement inaccuracies. In addition, the vertical and spatial accuracy of the DTM (Sect. 3.2.3) should be considered as it is an element of uncertainty. Thus, strike and dip values provide additional information of the internal geometry of ILDs, but should not be overestimated.

Thickness

To develop thickness profiles, the thickness is measured at locations where contour lines run parallel to the layering. For regions that exhibit several ILDs of the same morphology, exemplary profiles were generated. Assuming that layering is horizontal, thickness corresponds to the elevation difference (Fig. 26). As strike and dip measurements were only performed on ILDs with appropriate layering, as mentioned above, slightly inclined layers lower the accuracy of the measurement.

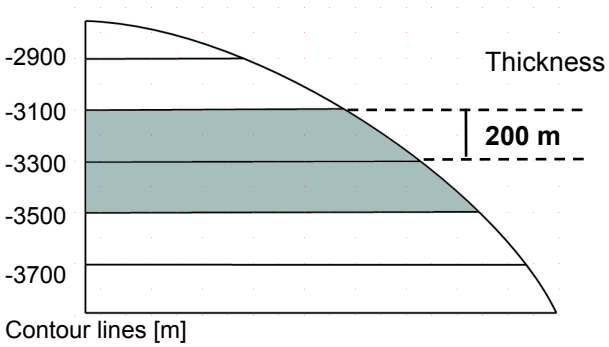


**Figure 26:** Example of how the thickness was measured. Appropriate candidates for thickness measurements are scarps that show distinct layering parallel to the contour lines. The measurement is then performed perpendicular to the contour lines and is equal to the elevation difference between top and bottom edge of the layer. Thickness measurements would be accurate to ±12.5 m for a 50 m/px HRSC-DTM with a corresponding nadir image of 12.5 m/px resolution (Sect. 3.1.1, Table 8).

Slope

HRSC and MOLA topography data were used to create slope maps. MOLA is employed in regions not covered by high-resolution HRSC DTMs. Slope maps are useful to demonstrate the distribution of steep and less steep parts across the ILD.

The slope angle is important for deducing the presence of rock and its properties (e.g. erosion) because the intensity of erosion depends on the slope angle. As the slope angle increases, erosion increases almost exponentially.

A slope line ($m$) in the plane containing x and y axes is defined by the changes in the y and the corresponding x-coordinate (Fig. 27) in two distinct points on the line, as described by:

$$m = \frac{\Delta y}{\Delta x} \qquad \text{(VI)}$$

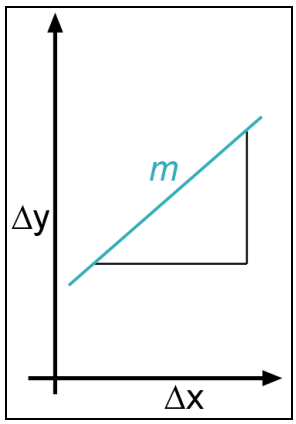


**Figure 27:** Slope angles are derived from the relationship between topography differences and the interpolated plane. The change in x (Δx) is expressed from one point to another by $x_2$-$x_1$ and for Δy by $y_2$-$y_1$. The accuracy is dependent of the DTM (Table 8). For a 50 m/px DTM x is ±50 m and y ±12.5 m for a corresponding nadir image with a resolution of 12.5 m/px (Sect. 3.2.3, Table 8).

Area and Volume

The heavily eroded nature of ILDs suggests they had a much greater extent in former times, which can be observed if several exposures exist in a given location. Such area and volume information is useful in estimating their complete extent before erosion.

Volume measurements were made to determine on what scale the ILD material was produced.

HRSC DTMs (Table 8) were applied to single ILDs and MOLA DEMs to entire areas. To work with the DLR's VICAR and IDL software, the extent of the area has to be defined first. Then the volume below a plane of a certain elevation is calculated and elevation differences on the plane are interpolated.